ELSEVIER

Journal of Applied Geophysics 32 (1994) 11–32

APPLIED GEOPHYSICS

Magnetic anomalies due to pyrrhotite: examples from the Cobar area, N.S.W., Australia

D.A. Clark, C. Tonkin*

CSIRO Division of Exploration Geoscience, P.O. Box 136, North Ryde, N.S.W. 2113, Australia

(Accepted after revision November 13, 1992)

Abstract

Rocks and ores containing monoclinic pyrrhotite are generally characterised by relatively intense remanence, which may be oblique to the present field direction, and high Koenigsberger ratios. Remanence should therefore be considered when interpreting magnetic anomalies due to pyrrhotite. Remanent magnetisation carried by pyrrhotite is readily reset by medium to low grade thermal events, but can be quite stable at ambient and slightly elevated temperatures. Palaeomagnetic studies of pyrrhotite-bearing units provide useful information on thermal history. Preferred orientation of pyrrhotite produces substantial susceptibility anisotropy that reflects the geological structure and which may sometimes be important for magnetic modelling. These points are illustrated by two case histories from the Cobar area: a stratigraphic horizon with disseminated monoclinic pyrrhotite (Magnetic Ridge) and a pyrrhotite-rich sulphide orebody (Elura).

1. Introduction

The crystallography and mineralogy of the pyrrhotite group have been reviewed by Ward (1970), Ribbe (1974), Shuey (1975), Power and Fine (1976) and Vaughn and Craig (1978). The general formula of pyrrhotites is $Fe_{1-x}S$, with $0 \leq x \leq 0.13$. Crystal structures in the pyrrhotite group are all superstructures of the NiAs structure. At elevated temperatures, above 300°C, Fe vacancies in the structure are disordered and the $Fe_{1-x}S$ solid solution adopts the hexagonal NiAs structure, which is denoted 1C. At lower temperatures the random distribution of vacancies gives way to various vacancy ordering schemes (depending on composition and thermal history) accompanied by formation of superstructures, usually with a lowering of crystal symmetry. The only common pyrrhotite type that is ferrimagnetic at ambient temperatures is monoclinic pyrrhotite with 4C superstructure and approximate composition Fe_7S_8. The ferrimagnetism of monoclinic pyrrhotite arises from the ordering of Fe vacancies onto alternate, antiferromagnetically coupled layers of Fe atoms. The spontaneous magnetisation of monoclinic pyrrhotite is ~90 G (90 kA/m) and its Curie temperature is ~320°. The spontaneous magnetisation is confined to the basal plane, except at cryogenic temperatures, by strong magnetocrystalline anisotropy. Within the basal plane there is also substantial intrinsic anisotropy, which controls magnetic domain structure and structure dependent properties such as susceptibility, remanence intensity and stability of remanence. Other common types, such as 5C pyrrhotite with composition ~Fe_9S_{10} and 6C pyrrhotite (~$Fe_{11}S_{12}$), are antiferromagnetic at room temperature. The temperature dependence of crystal structure of pyrrhotite is very sensitive to composition. The var-

*Present address: Westpac Project and Advisory Services Ltd., Level 28, 52 Martin Place, Sydney 2000, Australia.

0926-9851/94/$07.00 © 1994 Elsevier Science B.V. All rights reserved
SSDI 0926-9851 (94)00009-D

iation of magnetic properties with temperature is therefore diagnostic of composition. Thermomagnetic analysis of pyrrhotites has been discussed at length by Schwarz and Vaughan (1972).

Monoclinic pyrrhotite with composition $\sim Fe_7S_8$ is a relatively common ferrimagnetic mineral, particularly in areas with sulphide mineralisation. The magnetic susceptibility of monoclinic pyrrhotite is less than that of magnetite but is nevertheless substantial and strongly dependent on grain size. The susceptibility of monoclinic pyrrhotite decreases monotonically with decreasing grain size from ~0.1 G/Oe (1.3 SI) for very coarse ($\gtrsim$1 mm) grains, ~0.025 G/Oe (0.31 SI) for ~80 μm grains, 0.01 G/Oe (0.13 SI) for ~10 μm grains, to ~0.004 G/Oe (0.05 SI) for single domain ($\lesssim$2 μm) grains (Clark, 1983). The grain size dependence of magnetic hysteresis properties of natural pyrrhotites has been studied by Clark (1983, 1984) and Dekkers (1988).

Rocks and ores containing monoclinic pyrrhotite often carry relatively intense remanent magnetisation, characterised by Koenigsberger ratios greater than unity (Kropacek, 1971; Kropacek and Krs, 1971; Schwarz, 1974). Clark (1983) has shown that strong specific remanent intensities, high coercivity and high Koenigsberger ratios are predictable consequences of the intrinsic properties of monoclinic pyrrhotite, in particular the moderately high spontaneous magnetisation and the strong magnetocrystalline anisotropy. Theoretical, experimental and petrophysical studies have demonstrated that remanence carried by monoclinic pyrrhotite, particularly by fine grains, is magnetically hard and can be stable for geologically long periods at low temperatures (Clark, 1983). Remanence carried by monoclinic pyrrhotite is easily thermally reset, however, because of the low Curie temperature and the instability of the monoclinic phase with respect to antiferromagnetic pyrrhotite phases + pyrite above ~250°C. It is quite common, therefore, for pyrrhotite-bearing rocks to have a magnetisation dominated by an ancient remanence, which dates from the last significant thermal event(s) experienced by the rocks and which may be highly oblique to the present field. Interpretation of magnetic anomalies associated with such rocks may be seriously in error if the effects of remanence are ignored. Because of the high intrinsic anisotropy of monoclinic pyrrhotite, any preferred orientation of pyrrhotite grains produces substantial susceptibility anisotropy of the rock or ore within which the pyrrhotite occurs. The effect of anisotropy on the magnitude and direction of induced magnetisation may also be significant for magnetic interpretation, particularly when the pyrrhotite is coarse grained.

2. Geology of the Cobar area

The location of the Cobar Mining Field of central western New South Wales is shown in Fig. 1. Baker (1978) has given a general description of the geology of the Cobar area. The deformed Early Devonian turbidites of the Cobar Supergroup host three main types of sulphide mineralisation: copper + gold-rich deposits southeast of the town; a copper + lead + zinc-rich deposit 10 km north of the town (CSA mine); and the silver + lead + zinc-rich Elura deposit 40 km north of Cobar (Glen, 1987). The distribution of rock formations and mines from the Great Cobar area to Elura is shown in Fig. 2. Sediments of the Cobar Supergroup unconformably overlie intensely deformed rocks of the Girilambone Group, a turbiditic sequence of pre-Middle Silurian age, and are overlain by a fluviatile sequence, the Late Devonian–Early Carboniferous Mulga Downs Group.

The mineral deposits are confined to the Cobar Supergroup and are preferentially located in the finer grained sediments. The two operating mines (CSA and Elura) occur within the thin-bedded carbonaceous siltstones and mudstones, with minor sandstones, of the CSA Siltstone, which lies in the upper part of the Lower Amphitheatre Group. Mineralisation occurs as steeply

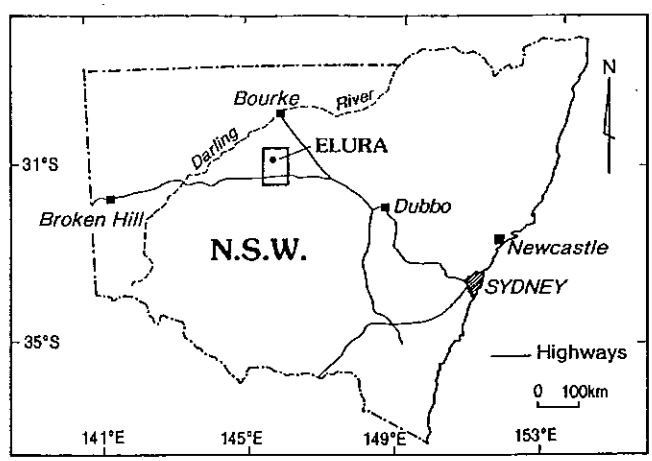

Fig. 1. Location of the Cobar Mineral Field.

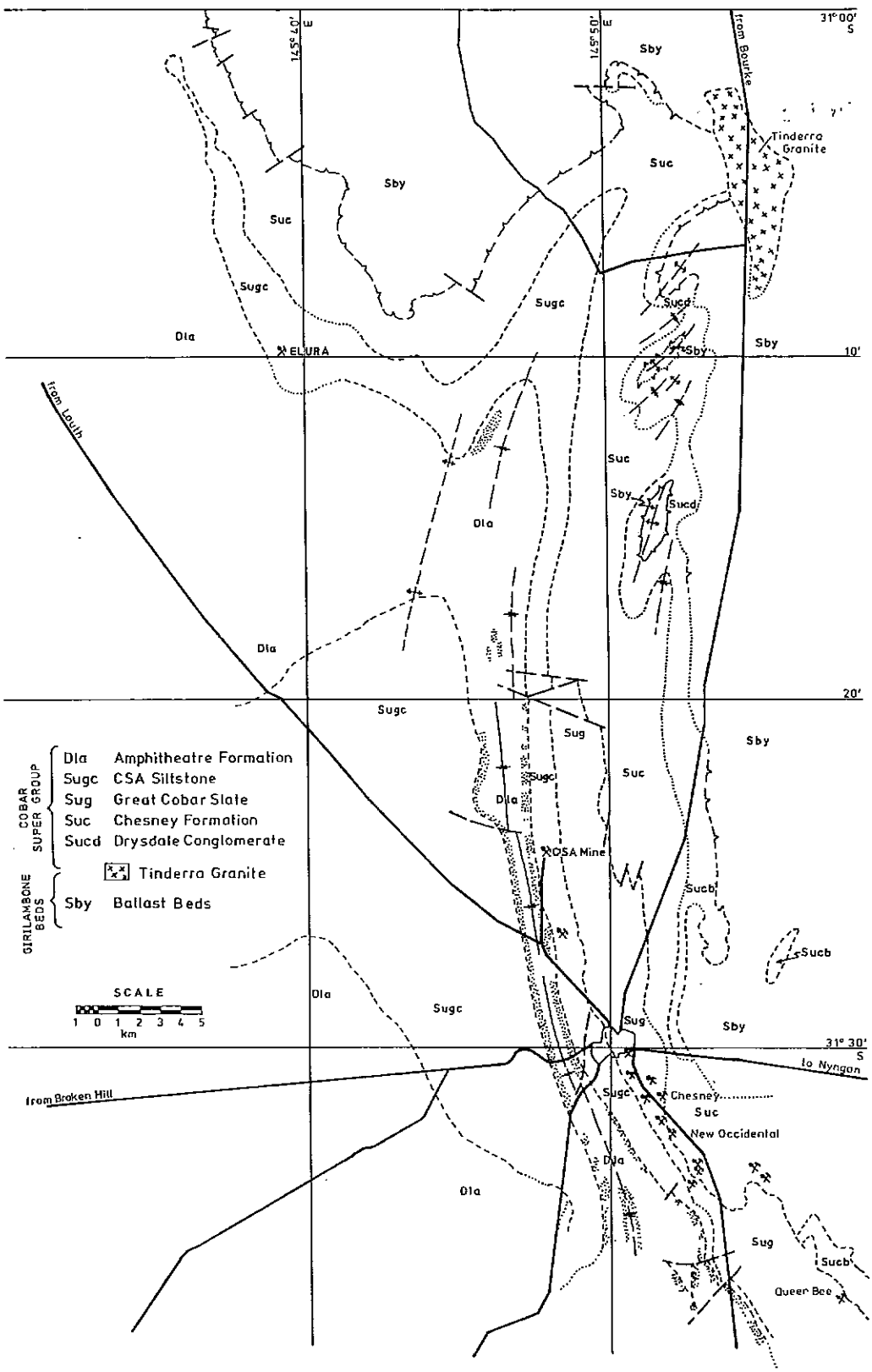

Fig. 2. Geology of the Cobar area, showing the major mines.

plunging, flattened, pipe-like bodies, which usually contain appreciable concentrations of pyrrhotite and/or magnetite. Because the ore bodies are usually associated with substantial magnetic anomalies, magnetic surveys are an important exploration tool in this area.

Rocks of the Cobar Supergroup were deformed and metamorphosed to lower greenschist grade in the Devonian and Carboniferous. The available evidence concerning the timing of deformation and metamorphism is equivocal and probably reflects a prolonged and complex thermal history. $^{40}Ar/^{39}Ar$ plateau ages of ~400 Ma from samples of the Great Cobar Slate and CSA Siltstone suggest that the main cleavage forming event, in part of the area at least, was Early Devonian, shortly after deposition (Glen et al., 1986). Determinations of metamorphic conditions indicate temperatures of ~350°C and average pressures of ~3 kbar, corresponding to a lithostatic load of ~11 km during metamorphism (Brill, 1988). The inferred pressures are about 1 kbar lower around Elura than for the area south of Cobar, indicating a higher geothermal gradient at Elura during metamorphism. The implication of the geobarometry is that the Cobar Supergroup was overlain by several kilometres of Mulga Downs Group sediments at the time of metamorphism and deformation. This supports a Carboniferous age for the deformation. An epidote (allanite) fission track age of 315 ± 27 Ma (Middle Carboniferous) from the Early Devonian Boolahbone Granite, which lies well to the south of Cobar, has been interpreted as a metamorphic age recording the deformation/metamorphism of the Cobar Supergroup (Pogson and Hilyard, 1981). Apatite fission track ages from other Silurian and Devonian granites range from 150 to 200 Ma (Early Cretaceous–Early Jurassic). Apatite fission track dates record the time of cooling through the ~100°C isotherm and the Mesozoic ages probably reflect final uplift and exposure of the area. The uplift may be associated with isostatic adjustment during the subsidence of the Great Australian Basin, which lies to the north.

3. The Magnetic Ridge anomaly

The Magnetic Ridge magnetic anomaly is a linear positive magnetic feature with a typical width of 500–1000 m and a maximum amplitude of ~50 nT, extending from 10 km south of Cobar to 20 km north of the CSA mine. The anomaly overlies part of the CSA Siltstone and is parallel to the stratigraphy. Magnetic Ridge and a number of similar magnetic features in the Cobar area coincide with lines of mineralisation and are therefore of exploration interest. A contour map from a regional aeromagnetic survey, depicting the Magnetic Ridge anomaly between Great Cobar and the CSA mine, is shown in Fig. 3.

The Australian Bureau of Mineral Resources, Geology and Geophysics (BMR) has investigated the Magnetic Ridge anomaly through aeromagnetic and ground magnetic profiles and a vertical hole drilled to a depth of 148 m (Hone and Gidley, 1986). The hole was centred on the local magnetic high within the Magnetic Ridge trend (Fig. 3). The rocks intersected in the drill hole comprise thin interbeds of detrital suspension-current siltstone and impure calcareous quartzite, partly of chemical sedimentary origin. The rocks were weathered down to the water table at a depth of ~100 m. Beneath the base of oxidation the rocks contain up to 1% pyrrhotite. Within the siltstone the pyrrhotite is preferentially concentrated along the incipient slaty cleavage, which dips steeply to the east, slightly oblique to the steeply westward dipping bedding planes. Calcareous quartzite layers preferentially host large diagenetic pyrrhotite grains.

Magnetic susceptibility measurements were made at 0.1 m intervals down the hole. The susceptibility of the weathered rocks in the depth interval 0–96 m is very low (~15 μG/Oe = 190×10^{-6} SI) and the *NRM*s are very weak (intensities of 0.1–10 μG or mA/m) and randomly directed. The average susceptibility of the unweathered, pyrrhotite-bearing rocks from the depth interval 97–148 m is significantly higher (~65 μG/Oe = 820×10^{-6} SI). This susceptibility is still quite low, and these rocks would generally be classified on the basis of their susceptibility as weakly magnetic. Drill core samples were taken at 5 m intervals down the hole for measurement of natural remanent magnetisation (*NRM*). Because the samples were azimuthally unoriented the declination of the remanence could not be determined, but the *NRM*s were found to be consistently upward directed. The average inclination of the *NRM* is −59°. The average *NRM* intensity is 165 μG (165 mA/m), which corresponds to a Koenigsberger ratio (Q) of ~4.4.

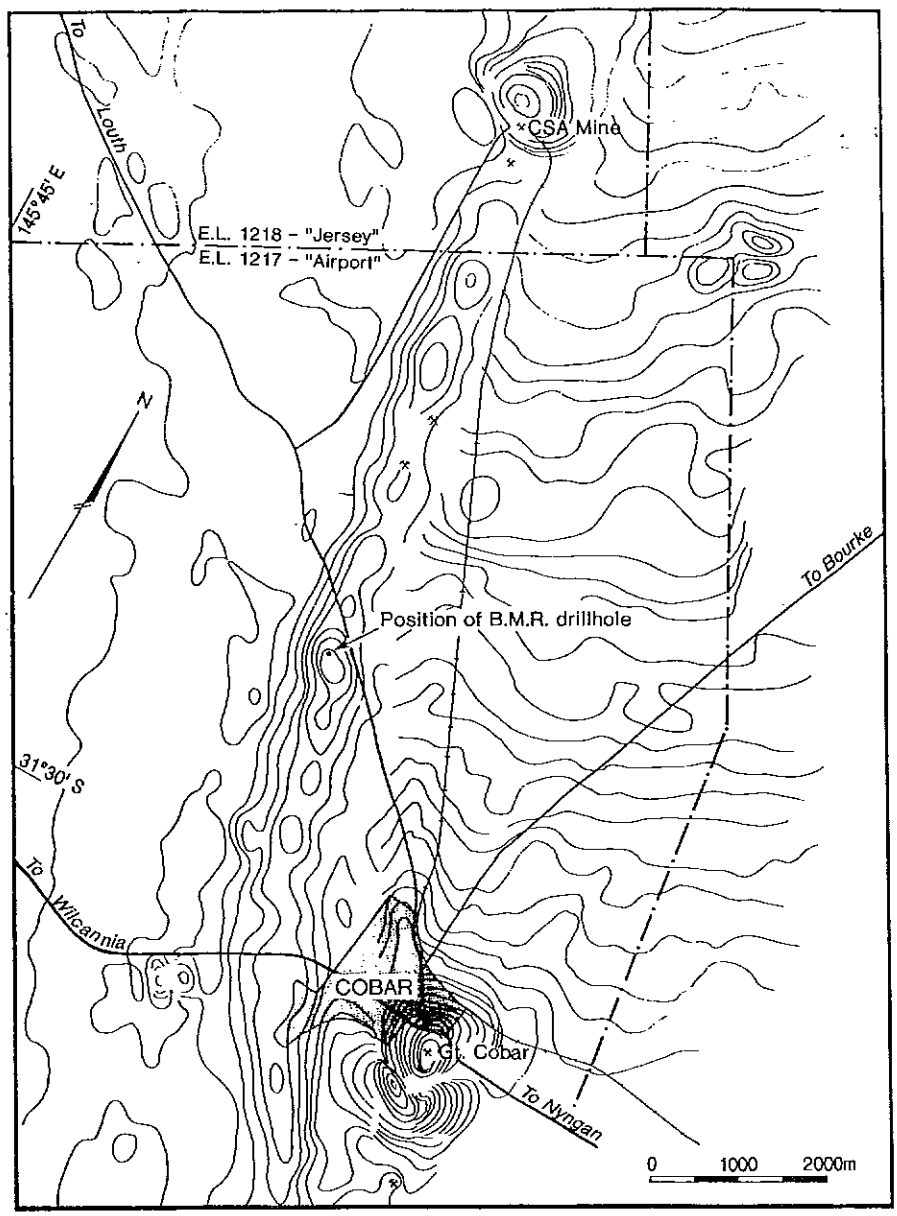

Fig. 3. Regional aeromagnetic contours of the Cobar area, showing the Magnetic Ridge anomaly. The contour interval is 5γ.

4. Magnetic properties of oriented samples

Detailed aeromagnetic contours over the Magnetic Ridge feature are shown in Fig. 4. In 1980 CRA Exploration Pty. Ltd. drilled an inclined hole, DD80 MR2, into the CSA Siltstone beneath the same magnetic feature targetted by the BMR. This hole, which was targetted on the interpreted source of the most prominent anomaly within the Magnetic Ridge trend, was 459 m long and intersected a sequence of graded siltstones and interbedded shale and siltstone units, with minor massive siltstone and sandstone units. A 300 m thick stratigraphic interval was intersected by the hole. Pyrrhotite was absent or rare from the rocks within 140 m of the surface. The hole intersected an interval containing minor pyrrhotite (~1%) between down-hole depths of 150 and 220 m, a zone of increased pyrrhotite (~2%) from 220 to 390 m, and a return to ~1% pyrrhotite from 390 m to the end of the hole. The pyrrhotite contents of the rocks are reflected in the susceptibility log (Fig. 5). The log shows a background susceptibility of ~40 μG/Oe (500×10^{-6} SI) for

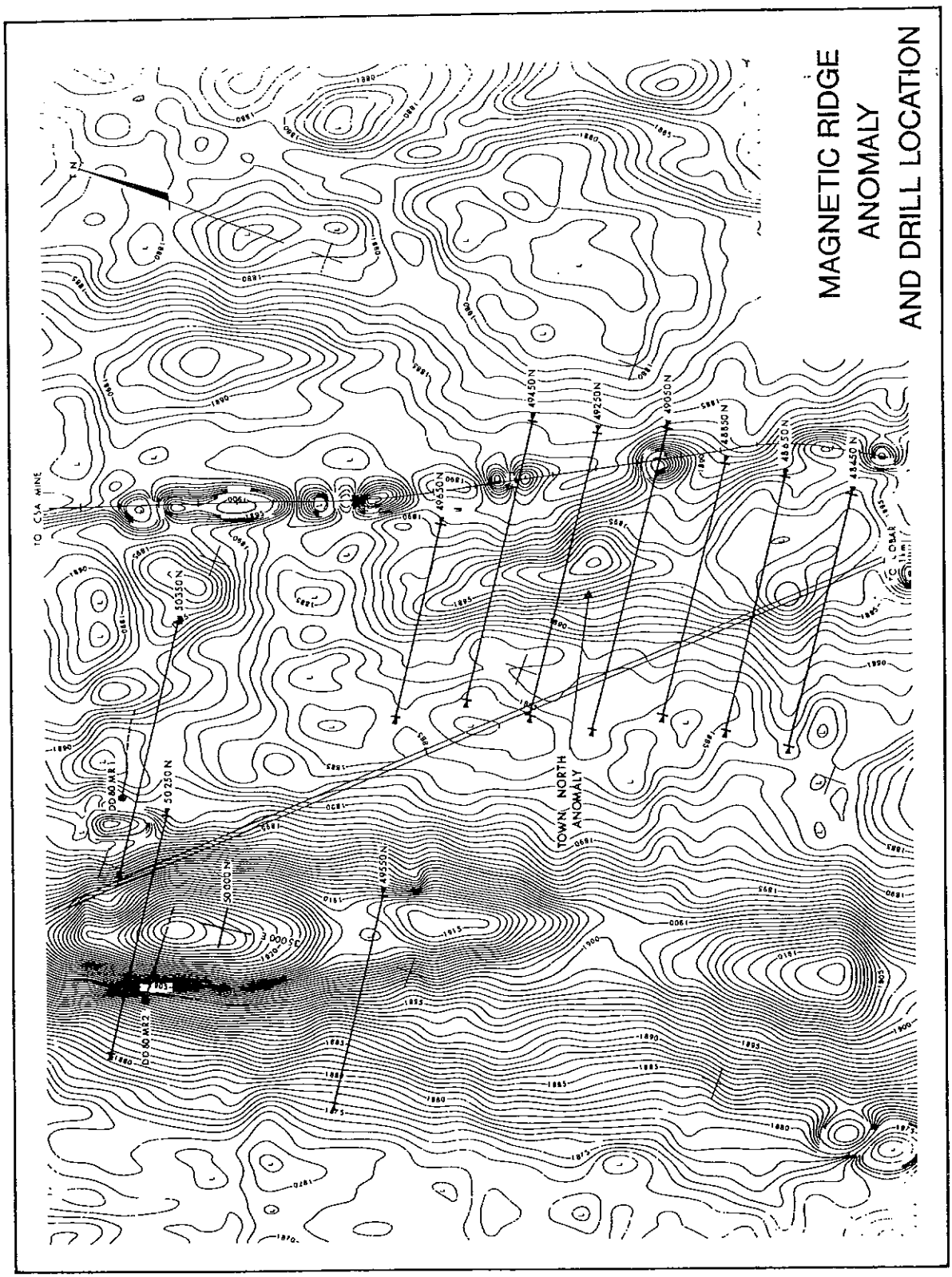

Fig. 4. Detailed aeromagnetic contours of the Magnetic Ridge area, showing the location of diamond drill hole DD80 MR2. As a guide to the sensitivity of the survey, note the distinctive line of anomalies associated with the Cobar–CSA mine railway track. Sensor terrain clearance was 40 m and the line spacing was 200 m. The contour interval is 1 γ.

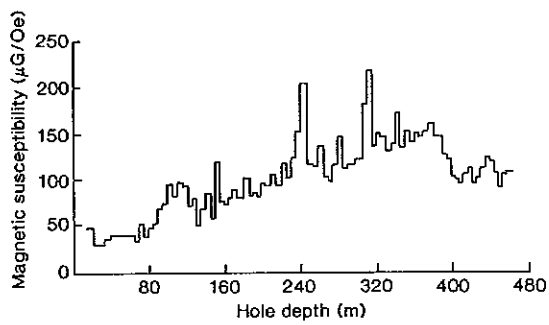

Fig. 5. Susceptibility log of hole DD80 MR2. The vertical scale is in μG/Oe.

weathered rocks; an average susceptibility of ~70 μG/Oe (880×10^{-6} SI) in the interval 90–150 m, similar to the susceptibility over the same depth interval in the BMR hole; an average susceptibility of ~100 μG/Oe (1260×10^{-6} SI) in the minor pyrrhotite zones; and the highest susceptibility (~140×10^{-6} μG/Oe = 1760×10^{-6} SI) in the zone of higher pyrrhotite concentration.

The measured susceptibilities are insufficient to account for the anomaly observed over this stratigraphic interval, particularly if the minor pyrrhotite zone is representative of the general pyrrhotite concentration within the CSA Siltstone at depth. In this case the susceptibility contrast between the narrow stratigraphic interval with enhanced pyrrhotite and the country rocks with the background pyrrhotite concentration is only ~40 μG/Oe (500×10^{-6} SI), which is too small by an order of magnitude to account for the anomaly. Even if the pyrrhotite is restricted entirely to the intersected interval and the surrounding rocks are assumed to have zero susceptibility, the anomaly arising from induced magnetisation of the pyrrhotitic zone would be smaller than the observed anomaly by a factor of ~4. This suggests either that the true source of the anomaly was not intersected or that remanent magnetisation of the intersected units is predominantly responsible for the magnetic signature. It was important to ascertain whether the disseminated pyrrhotite horizon accounted for the anomaly, because the alternative possibility of another, unintersected, source might represent an orebody.

The bedding attitude is very consistent over most of the intersected stratigraphic interval. Because the inclined hole was drilled orthogonal to the geological strike and intersected the very steeply W-dipping beds obliquely, it was possible to orient drill core samples azimuthally by aligning the clearly visible bedding laminations in the cores with the known bedding attitude. Combined with the drill hole survey, this allowed unique orientations to be obtained for core samples.

CRA Exploration Pty. Ltd. supplied six orientable samples from the enhanced pyrrhotite zone for determination of magnetic properties. These samples were redrilled along their axes and then sliced into standard 2.5 cm diameter × 2.2 cm height palaeomagnetic specimens. The bulk susceptibilities were measured using a transformer bridge developed by the CSIRO (Ridley and Brown, 1980) and the remanence vectors were measured on a Digico fluxgate spinner magnetometer. A Digico anisotopy delineator was used to measure susceptibility anisotropy. The susceptibilities, *NRM* intensities and directions, and Koenigsberger ratios of these samples are given in Table 1. The susceptibilities are relatively consistent, with a range of 70–180 μG/Oe (880–1130×10^{-6} SI) with an average of 110 ± 14 μG/Oe (1380×10^{-6} SI). The *NRM* intensities and Koenigsberger ratios are much more variable. The *Q*-values are all greater than unity, ranging from 2 to 24, suggesting that remanence dominates the magnetisation of these rocks. The *NRM* data in Table 1 is presented in a conventional form, with the sample *NRM* given as the arithmetic mean ($\pm$ the standard error) of the specimen intensities and the sample *NRM* direction calculated as the mean of the specimen directions, each with unit weight. It will be shown below that this is not the most appropriate characterisation of the bulk remanence properties for petrophysical purposes (as opposed to palaeomagnetic studies), although in the present case it is adequate for semiquantitative discussion.

The samples have a well-defined magnetic fabric, with tightly clustered principal susceptibility axes. The major susceptibility axes (magnetic lineations) and minor susceptibility axes (magnetic foliation poles) are plotted in Fig. 6. The magnetic foliation, which is the plane of relatively high susceptibility containing the major and intermediate axes and normal to the cluster of minor axes, dips steeply E, parallel to the cleavage. Within this plane the magnetic lineations plunge steeply to the NE, subparallel to the steeply plunging regional mineral and extension lineations in these rocks. The average anisotropy magnitude (major susceptibility/minor susceptibility) of 31 specimens is

1.45 ± 0.02. The preferred orientation of pyrrhotite grains in the cleavage suggests a pre- or syndeformational formation of the pyrrhotite. Thermomagnetic analysis of sample 310.4 m showed that monoclinic pyrrhotite was the only ferrimagnetic mineral present in detectable quantity. The magnetic properties are therefore associated with monoclinic pyrrhotite, with negligible contributions from other ferrimagnetic minerals.

Closer examination of the data in Table 1 reveals that the samples fall into two categories:

(1) Samples with relatively high Koenigsberger ratios ($Q > 10$) and consistent *NRM* directions for all specimens cut from the core (e.g. sample 250.0 m). *NRM* directions of specimens from these samples are all of normal polarity for the southern hemisphere, with steep negative inclinations.

(2) Samples 270.5 and 310.4 m which have relatively low *NRM* intensities and Koenigsberger ratios ($Q < 4$). *NRM* directions of specimens from these samples are streaked, approximately along a great circle, suggesting the presence of varying proportions of two highly oblique remanence components.

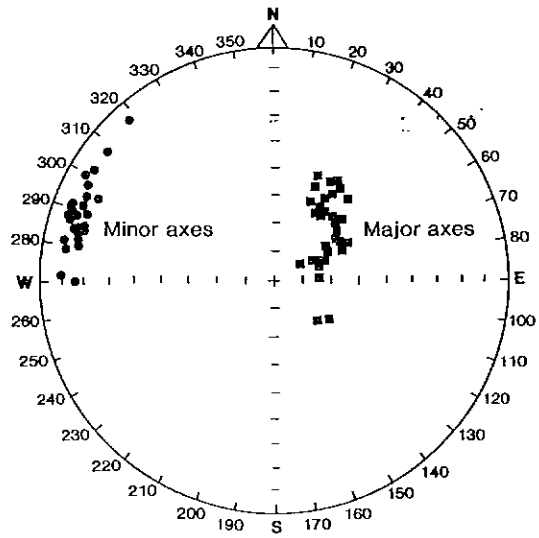

Fig. 6. Magnetic fabric of the Magnetic Ridge samples. The dots represent minor susceptibility axes (magnetic foliation poles) and the squares represent major susceptibility axes (magnetic lineations). Equal area, lower hemisphere projection (Schmidt net).

The *NRM* directions of specimens from samples 250.0, 270.5 and 310.4 m are plotted on a stereonet in

Table 1
Magnetic properties of Magnetic Ridge samples from CRAE hole DD80 MR2

Sample	N	$\bar{k}$ (Range)	$\bar{J}$ (Range)	(D, I) (α_{95})	Components	$\bar{Q}$
250.0 m	5	90 ± 20 (60–170)	850 (490–1810)	(257°, −66°) (3°)	*SN* + *HN*	16 ± 1
270.5 m	4	90 ± 20	100 (30–210)	(286°, +23°) (269°, −03°)–(289°, +55°)	*SN* + *HR*	1.0 ± 0.3
291.8 m	7	70 ± 10	480 ± 120 (230–920)	(252°, −55°) (5°)	*SN* + HN	11 ± 1
310.4 m	7	180 ± 30 (60–250)	370 ± 60 (120–600)	(269°, +09°) (271°, −27°)–(297°, +77°)	SN + *HR*	3.6 ± 0.2
340.3 m	6	135 ± 20 (80–220)	1950 ± 410 (1050–3710)	(239°, −51°) (6°)	*SN* + *HN*	24 ± 2 15.3 ± 0.5
344.5 m	7	96 ± 6	850 ± 60 (610–1070)	(237°, −56°) (6°)	*SN* + *HN*	

N = No. of specimens cut from drill core sample.
$\bar{k}$ = Mean susceptibility in μG/Oe (1 μG/Oe = 12.56 × 10^{-6} SI).
$\bar{J}$ = Mean *NRM* intensity in μG (1 μG = 1 mA/m).
$\bar{Q}$ = Mean Koenigsberger ratio ($Q = J/kF$), where $F = 0.575$ Oe (= 57500 nT) in Magnetic Ridge area.
D = Declination of mean *NRM* direction (positive clockwise from *TN*); I = Inclination of mean *NRM* direction (positive downward). The mean *NRM* direction is calculated giving unit weight to specimen *NRM* directions.
α_{95} = Radius of 95% circle of confidence about mean *NRM* direction, for well grouped directions. For the samples with *SN* + *HR* components the *NRM* directions of individual specimens are streaked along a girdle stretching between the indicated extreme directions.
The arithmetic mean value ± the standard error of the mean is given if values from individual specimens are well grouped, otherwise the range of values is shown.
SN = Soft normal remanence component; *HN* = hard normal remanence component; *HR* = hard reversed remanence component.

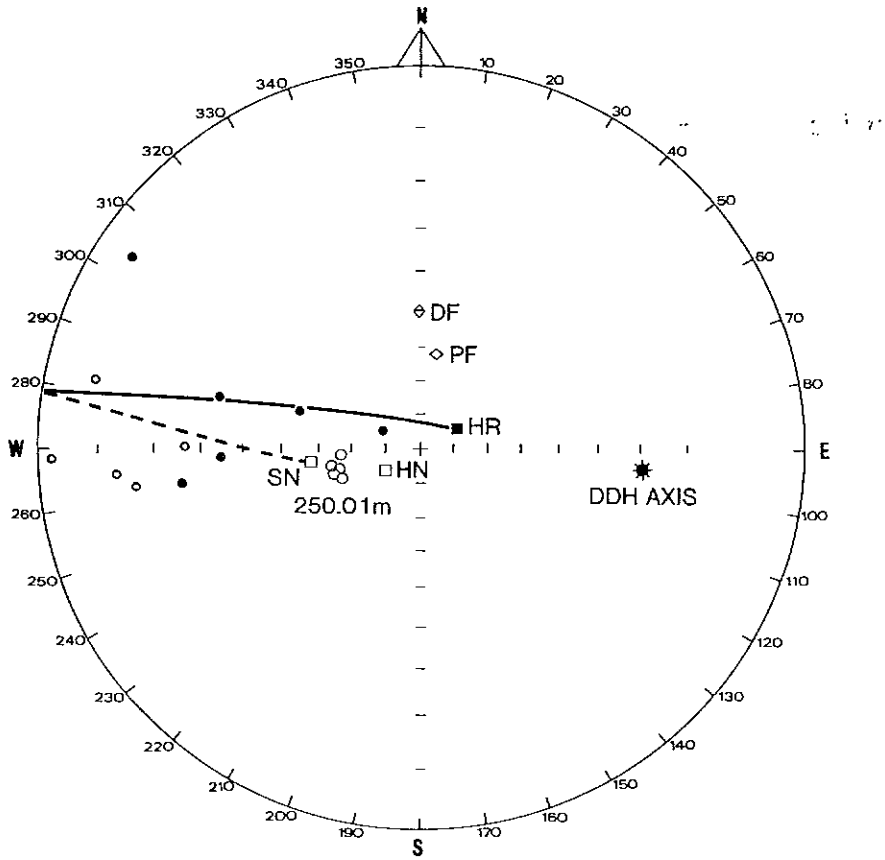

Fig. 7. *NRM* directions of specimens from sample 250.0 m (larger circles), with soft normal + hard normal components, and samples 270.5 and 310.4 m (smaller circles and dots), with soft normal + hard reversed components. *DF* = geocentric axial dipole field, *PF* = present field, *SN* = mean direction of soft normal components, *HN* = mean direction of hard normal components, *HR* = mean direction of hard reversed components (antiparallel to *HN*, within experimental error). In this, and all subsequent, stereonets open symbols are on the upper hemisphere and closed symbols are on the lower hemisphere.

Fig. 7. Standard palaeomagnetic cleaning techniques were applied to specimens from all samples in order to characterise the remanence components present in each sample. Readers unfamiliar with palaeomagnetic laboratory techniques and methods of presentation and analysis of palaeomagnetic data are referred to the book of Collinson (1983). Alternating field and thermal demagnetisation gave similar results. In all samples the *NRM* was found to comprise two distinct components: a relatively soft component of normal polarity (*SN*), with moderate negative inclination, overprinting a very steep harder component, which may have either polarity. Type (1) samples have hard components with normal polarity (*HN*), which are subparallel to the soft component and augment the *NRM* intensity and *Q*-value. Type (2) samples, on the other hand, have hard components with reversed polarity (*HR*), which oppose the dominant soft component, thereby reducing the *NRM* intensities and *Q*-values of these samples.

The soft and hard components have fairly discrete stability characteristics: the soft component only is removed by AF demagnetisation to 50–100 Oe (5–10 mT) and thermal demagnetisation to ~150°C. The hard component is consistently removed by AF treatment above 100–150 Oe AF and thermal demagnetisation above 150–180°C. Typical Zijderveld plots showing AF and thermal demagnetisation trends for type (1) and (2) samples are shown in Fig. 8. It can be seen from these plots that both the soft and hard components are well defined by linear segments and that the segment corresponding to the hard component heads directly towards the origin of the plots, indicating that it is well resolved and is the most stable component present in the samples. In all cases the remanence was

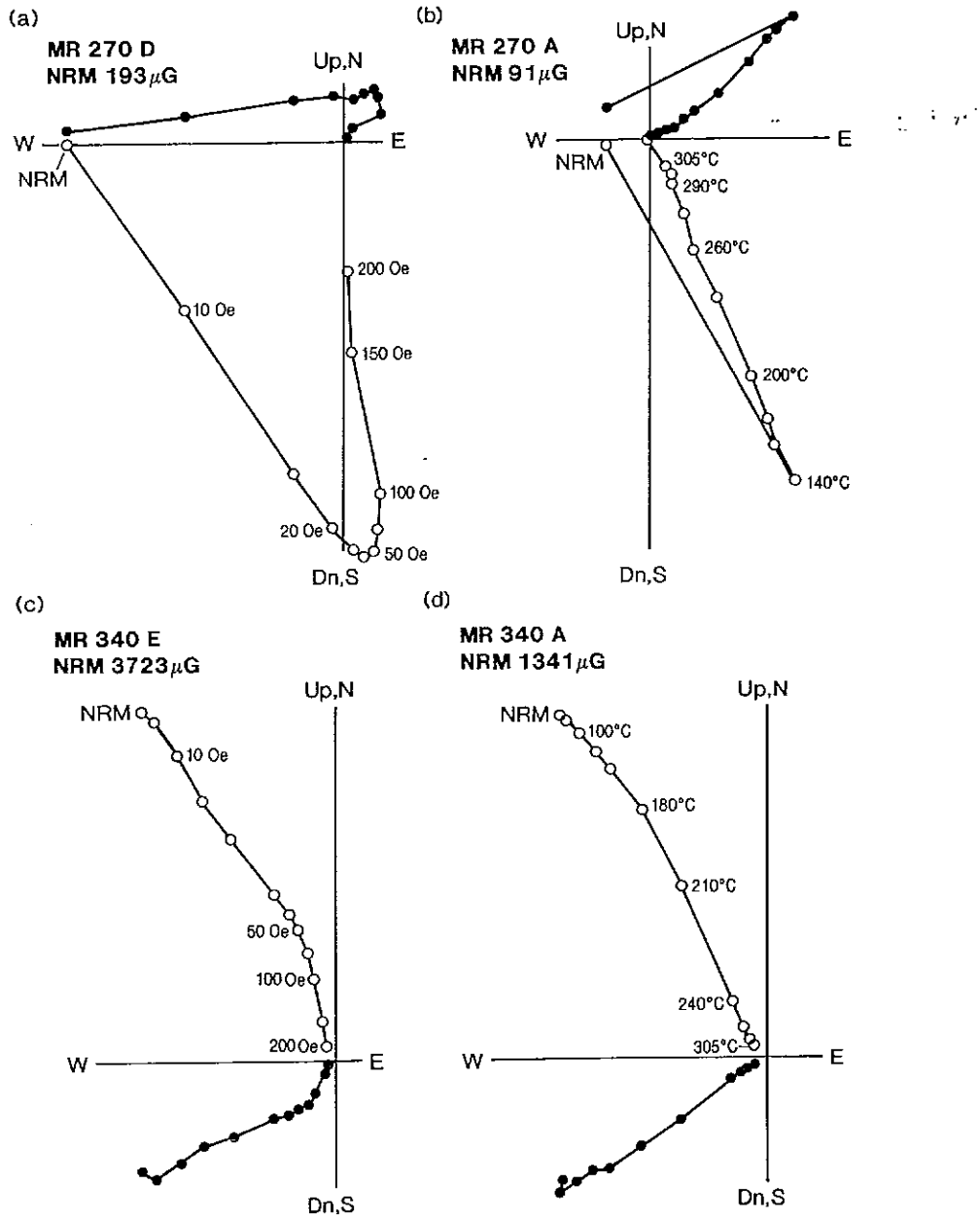

Fig. 8. Zijderveld plots for palaeomagnetic cleaning of specimens from Magnetic Ridge. (a) AF demagnetisation and (b) thermal demagnetisation of specimens from sample 270.5 m, showing a soft normal component overprinting a hard reversed component. (c) AF demagnetisation and (d) thermal demagnetisation of specimens from sample 340.3 m, showing the soft normal component overprinting a hard normal component that is antiparallel to the hard component in (a) and (b). The dots represent the projections of successive remanence vector end-points onto the horizontal plane. The open circles represent the corresponding projections onto the E–W vertical plane.

completely demagnetised above ~310°C, indicating that pyrrhotite carries the remanence.

Fig. 9 shows successive measured remanence directions (M) and directions of the subtracted vector (S) after each AF demagnetisation step for a specimen with soft normal + hard reversed components, which combine to produce an *NRM* which is directed W and horizontal. As the soft component is preferentially removed the remanence moves along a great circle, away from the initial horizontal direction, towards the stable end point corresponding to the steep down hard component. The directions of the vectors removed by

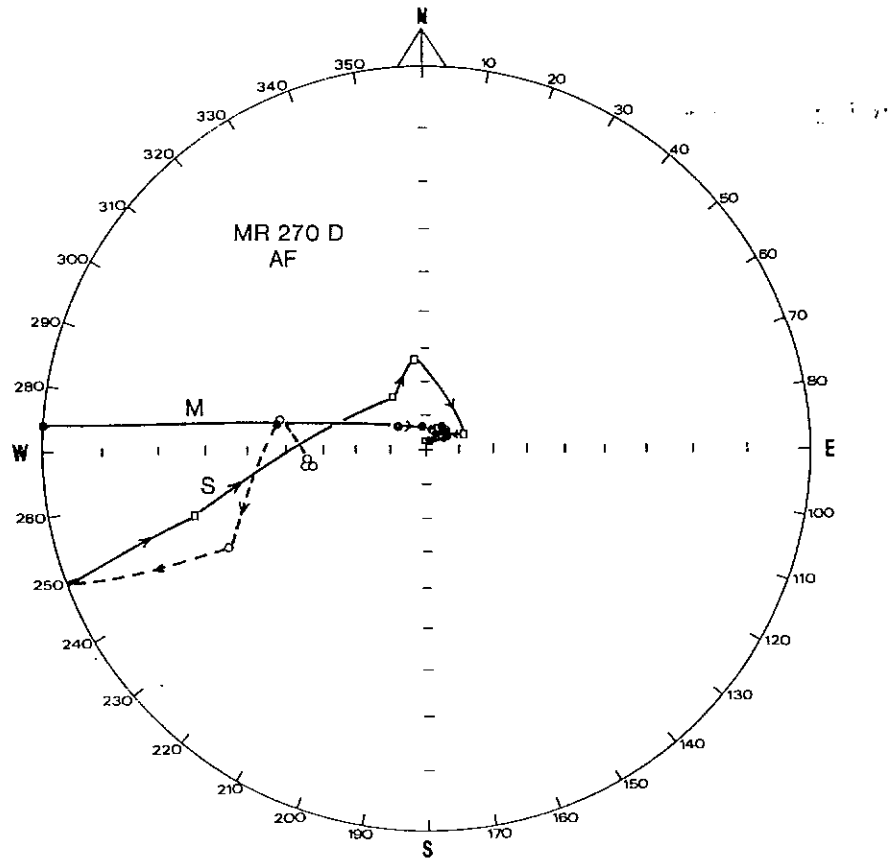

Fig. 9. Directions of successive measured remanence vectors (M), and successive subtracted vectors (S), during stepwise AF demagnetisation of the specimen for which the Zijderveld plot is shown in Fig. 8a. Equal-angle stereographic projection, referred to geographic north.

successive demagnetisation treatments initially coincide with the soft normal component, then move along the same great circle trend, until the direction of the hard component is attained.

The demagnetisation data were analysed using Principal Component Analysis (Kirschvink, 1980) and the directions obtained from the best-fit linear segments were combined to calculate mean directions for the soft and hard components. The soft component (SN) has mean direction $D=263°$, $I=-58°$ ($N=36$, $K=13.3$, $\alpha_{95}=7°$). Here, N is the number of specimens for which the soft components were defined; K is Fisher's (1953) precision parameter; and α_{95} is the radius of the 95% cone of confidence about the mean direction. The hard components (HN and HR), after conversion of reversed directions to normal polarity, have mean direction $D=238°$, $I=-78°$ ($N=36$, $K=8.5$, $\alpha_{95}=9°$). The mean direction of the soft component and both polarities of the mean hard component are plotted in Fig. 7, which shows clearly why samples with subparallel $SN+HN$ components have specimens with well clustered NRM directions lying between the SN and HN mean directions, whereas samples with $SN+HR$ components have a girdle distribution of specimen NRM directions.

Without the benefit of palaeomagnetic cleaning the rather large range in remanent intensities and Q-values of these samples and the scattered NRM directions would have caused difficulties for characterisation of the bulk magnetic properties of the magnetic source. There are no rigorous methods available for estimation of mean remanence vectors, with confidence intervals, when there is great variability in magnitude and direction. A further complication arises when the magnitude and direction of the remanence are correlated, as they are for these rocks. However, resolution of the rema-

nence vectors into two well-defined components allows estimation of the contributions of the soft and hard components separately.

The age of the remanence components cannot be determined unambiguously, because of ill-defined portions of the Late Palaeozoic–Mesozoic apparent polar wander path for Australia and because the track crosses over itself twice. Palaeomagnetic study of samples from another six drill-holes in the CSA Siltstone has shown the soft normal and hard normal components to be present throughout the adjoining areas (Clark, 1983). The most plausible interpretation of the components is that they represent regional low-grade thermal events. The mean direction of the hard components from seven different "sites", each representing a drill-hole, is $D=223°, I=-80°$ ($N=7, K=54.3, \alpha_{95}=8°$). The corresponding palaeopole position is 17°S, 159°E ($dp=15°, dm=16°$), where dp is the radius of the 95% oval of confidence along the palaeomeridian and dm is the radius orthogonal to the palaeomeridian. The mean direction of the soft components is $D=244°, I=-71°$ ($N=7$, $K=18.3$, $\alpha_{95}=15°$). The corresponding palaeopole is 12°S, 178°E ($dp=22°, dm=25°$). These palaeopoles lie close to the Late Palaeozoic–Mesozoic track of Embleton (1981). Based on the unblocking temperatures during thermal demagnetisation and the thermal activation nomograms of Clark (1983), the hard component probably records postmetamorphic cooling through the ~250°C isotherm in the Triassic and the soft component probably records cooling through the ~100°C isotherm during final uplift and cooling in the Middle Jurassic–Early Cretaceous.

5. Modelling the Magnetic Ridge anomaly

The measured magnetic properties indicate that remanence is the dominant contributor to the magnetisation and suggest that the anomaly arises from the distribution of disseminated pyrrhotite, rather than from an additional unintersected source. Because the total magnetic moment of a volume of rock is the vector sum of the magnetic moments of its subvolumes, the appropriate method for calculating the *NRM* vectors of a sample is to add the *NRM* vectors from its constituent specimens and divide by their number. This vectorial mean weights the contribution of each *NRM* according to its intensity, in contrast to estimation of mean palaeofield direction from a palaeomagnetic data set, which gives each direction unit weight. Similarly, estimation of the average remanence of a rock unit for modelling the associated magnetic anomaly requires calculation of the vectorial mean of the *NRM*s of samples from the unit.

Table 2
Mean remanence vectors of Magnetic Ridge samples

Sample	Intensity (μG)	Declination	Inclination
250.0 m	845	259°	−66°
270.5 m	90	281°	+12°
291.8 m	473	255°	−56°
310.4 m	326	268°	+04°
340.3 m	1940	240°	−53°
344.5 m	843	237°	−57°
Combined	710	248°	−53°

The mean *NRM* vectors of the oriented samples from Magnetic Ridge are given in Table 2. Comparison with the (scalar) mean intensities and the mean directions obtained by combining unit vectors in Table 1 reveals significant differences for the samples with *SN+HR* components. This arises because the *NRM*s of individual specimens reflect varying proportions of two oblique components. As a result the direction and intensity of the *NRM* from individual specimens are strongly correlated. Combining the sample *NRM*s of Table 2 to calculate the "formation mean" remanence vector for the magnetic horizon gives: $int=710$ μG, $D=248°$, $I=-53°$. Applying the same procedure to the incorrectly calculated "sample mean" *NRM*s of Table 1 gives a very similar result for the estimated "formation mean", although the individual sample *NRM*s in Table 1 are biased estimates. This is because the "formation mean" *NRM* is dominated by the contribution of the relatively intense *SN+HN* samples, for which the "sample mean" intensities and directions of Table 1 are only slightly biased, whereas the highly biased, but relatively weak, sample *NRM*s of the *SN+HR* samples have lower weight. The "formation mean" direction, calculated with unit weight to samples from the directions listed in Table 2, is significantly shallower than the correctly calculated "formation mean" *NRM*, because the contribution of the *SN+HR* samples is overemphasised.

The geological and susceptibility logs suggest that the Magnetic Ridge anomaly is associated with a strat-

igraphic interval with a pyrrhotite content that is slightly elevated above a background level. This implies that the background magnetisation of the surrounding rocks should be taken into account, as magnetic anomalies arise from magnetisation contrasts rather than from absolute magnetisations. Because oriented samples were supplied only from the more magnetic zone the background properties of the surrounding rocks had to be estimated from their inferred pyrrhotite content, by assuming that the properties of the pyrrhotite grains are consistent throughout the section and that variations in the magnetic properties of the rocks reflect only differences in pyrrhotite concentration. The contribution of pyrrhotite to the susceptibility of the rocks can be deduced from the susceptibility log and the corresponding remanence can then be estimated from an empirical relationship between the remanence intensity and susceptibility of the core samples. The susceptibility k of a rock containing a volume fraction $f \ll 1$ of a ferrimagnetic mineral dispersed within a paramagnetic matrix can be modelled as the sum of the contributions from the ferrimagnetic and paramagnetic fractions:

$$k=(1-f)k_{\text{para}}+fk_{\text{ferri}} \approx k_{\text{para}}+fk_{\text{ferri}} \quad (1)$$

where k_{para} is the susceptibility of the paramagnetic minerals and k_{ferri} is the susceptibility of the ferrimagnetic mineral (both referred to unit volume). Only the ferrimagnetic mineral contributes to the remanence, however:

$$J=fQ_{\text{ferri}}k_{\text{ferri}}F \quad (2)$$

where J is the intensity of the remanence (which is assumed to be monocomponent), Q_{ferri} is the intrinsic Koenigsberger ratio of the ferrimagnetic mineral and F is the magnitude of the geomagnetic field. The Koenigsberger ratio of the rock is less than Q_{ferri} because of the paramagnetic contribution to the susceptibility:

$$Q=J/kF \approx Q_{\text{ferri}}/[1+k_{\text{para}}/fk_{\text{ferri}}] \quad (3)$$

Combining Eqs. (1) and (2) gives:

$$J \approx [k-k_{\text{para}}]Q_{\text{ferri}}F \quad (4)$$

Eq. (4) shows that there is a linear relationship between the remanence intensity and the susceptibility of the rock, that is effectively independent of the volume fraction of ferrimagnetic mineral for dilute dispersions. Plotting J vs. k for samples with varying ferrimagnetic mineral contents should therefore yield a straight line with slope equal to $Q_{\text{ferri}}F$ and intercept on the k-axis equal to k_{para}. This relationship is complicated by multicomponent remanence. In the case of the Magnetic Ridge samples, however, the $SN+HN$ and $SN+HR$ samples can be analysed separately to obtain estimates of the intrinsic Q-values of grains with two subparallel normal components and those with opposing components. The analysis above is based on the assumption that the average intrinsic properties of the ferrimagnetic grains are independent of their concentration. The linearity of the empirical relationship between J and k and the plausibility of the values for Q_{ferri} and k_{para} derived from this relationship provide tests of this assumption.

Calculation of a linear regression of J on k for the four $SN+HN$ samples gives $J=23$ $(k-53)$ with a correlation coefficient of 0.99. By comparison with Eq. (4), this implies $k_{\text{para}}=53$ μG/Oe and $Q_{HN}=23/0.58=40$, where Q_{HN} is the intrinsic Koenigsberger ratio of the grains carrying $SN+HN$ components. The slope and intercept of the line defined by the J and k values of the two $SN+HR$ samples similarly give $k_{\text{para}}=56$ μG/Oe and $Q_{HR}=4.5$. The remanence intensities and Koenigsberger ratios of the two types of sample can therefore be considered as arising from superposed soft and hard components with respective intrinsic Koenigsberger ratios $Q_{\text{soft}} \sim 22$ and $Q_{\text{hard}} \sim 18$ that add in the case of a normal polarity hard component and subtract in the case of a reversed hard component (neglecting the $\sim 20°$ angular difference between the SN and HN components).

Given the empirical relationship between J and k, the NRM of the zone of low pyrrhotite content can be predicted from the susceptibility log. The susceptibility due to the paramagnetic matrix is estimated to be ~ 50 μG/Oe, so that the disseminated pyrrhotite contributes ~ 40 μG/Oe to the total susceptibility of ~ 90 μG/Oe for the minor pyrrhotite zone and ~ 90 μG/Oe to the total susceptibility (~ 140 μG/Oe) of the enhanced pyrrhotite zone. Thus the pyrrhotite content of the minor pyrrhotite zone is about 4/9 of the concentration in the enhanced pyrrhotite zone. This suggests that the average NRM intensity in the minor pyrrhotite zone is $\sim 4/9 \times 710$ μG $\simeq 320$ μG and the remanence contrast between the magnetic zone and the surrounding rocks is ~ 390 μG. Because the average intrinsic properties

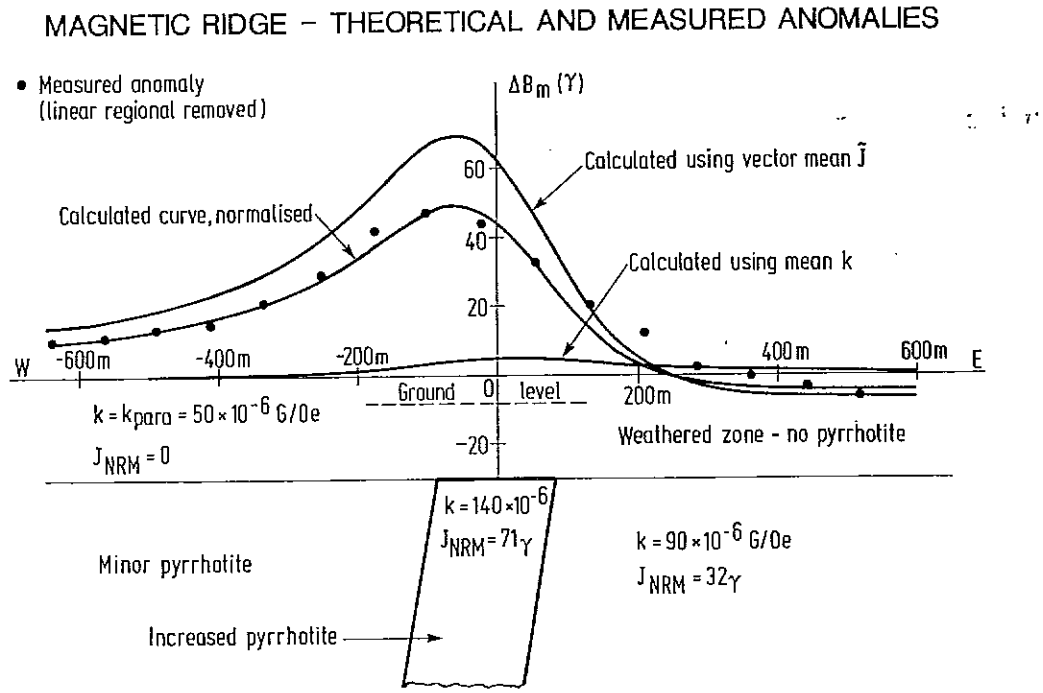

Fig. 10. 2-D magnetic model of the Magnetic Ridge anomaly, incorporating drilling information and the measured magnetic properties.

of the pyrrhotite are presumed to be the same inside and outside the most magnetic zone, the estimated direction of the background remanence and of the remanence contrast is the same as for the most magnetic zone, i.e. $D=248°$, $I=-53°$.

Since magnetic anomalies are expressed in terms of gammas (nT), it is convenient to also express magnetisations in gammas ($1\ \gamma=10^{-5}$ G $=10\ \mu$G) in order to calculate the theoretical anomaly arising from a given source geometry. The effective magnetisation (=magnetisation contrast) of the magnetic zone is then the vector sum of remanence with $int=39\ \gamma$, $D=248°$, $I=-53°$ and induced magnetisation, parallel to the present field, with $int=$kF$=50\times10^{-6}$ G/Oe$\times$57,500 $\gamma=2.9$ c, $D=9.5°$, $I=-62.5°$. The effective Koenigsberger ratio for the magnetic zone is therefore $39/2.9\simeq13$ and the total magnetisation is: $int=41\ \gamma$, $D=251°$, $I=-56°$. The small deflection of the induced magnetisation due to anisotropy is ignored here, because the effect of anisotropy is minor and is in any case swamped by the much larger contribution of remanence to the total magnetisation.

The 2-D magnetic model of Fig. 10 was based on this magnetisation contrast, with source geometry constrained by the geology and the drilling data. The thickness, dip, depth and location of the sheet-like body were based solely on the drilling. No attempt was made to improve the match between theoretical and observed anomalies by adjusting the model geometry or properties. The susceptibility measurements from the BMR and CRAE holes suggest that a horizontal layer with small amounts of pyrrhotite and susceptibility slightly above the paramagnetic background level, possibly increasing with depth as weathering effects decrease, should be inserted immediately above the magnetic body in Fig. 10. However, a laterally homogeneous layer produces no external magnetic field, so this zone can be omitted from the model.

The amplitude of the predicted anomaly is comparable to that of the residual observed anomaly, but is ~30% higher. This agreement is satisfactory, given the limited number of samples on which the estimate of representative magnetic properties is based and the simplicity of the assumed model. Normalising the anomaly amplitude by adjusting the intensity of the total magnetisation shows that the shapes of the theoretical and observed anomalies agree quite well. Ignoring the remanent magnetisation, on the other hand, gives a predicted anomaly that is much smaller than the actual anomaly. Thus, although the susceptibility of the magnetic zone cannot account for the Magnetic Ridge anomaly, when remanence is considered, it becomes

apparent that the anomaly is associated with the disseminated pyrrhotite horizon. There is therefore no evidence of any additional magnetic source and further expensive drilling in search of a possible economic sulphide orebody is not warranted. If the background magnetisation of the rocks surrounding the magnetic zone is ignored, the predicted anomaly exceeds the observed anomaly by a factor of ~ 2. This serves as a reminder that anomalies are associated with magnetisation contrasts, not absolute magnetisations. The Magnetic Ridge case history affords a good example of the utility of retrospective analysis of magnetic properties

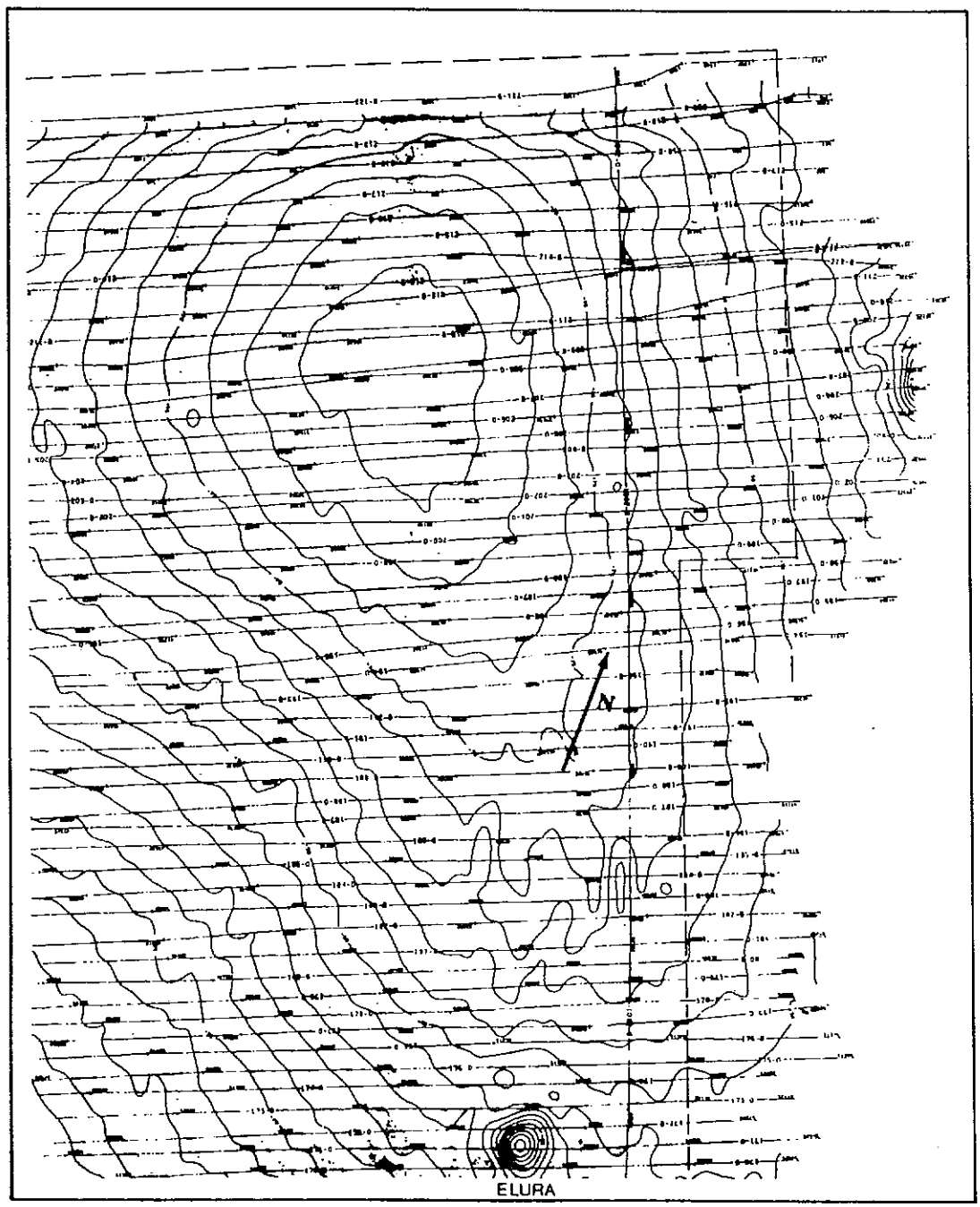

Fig. 11. Detailed aeromagnetic contours over Elura and the area to the north (from Emerson, 1980). The contour interval is 5γ. The survey terrain clearance was 90 m and the flight line spacing was 300 m.

in order to ascertain whether an anomaly has been adequately tested by drilling.

6. The Elura orebody

The Elura Zn–Pb–Ag deposit is located 43 km NNW of Cobar and is the northernmost known orebody in the Cobar Mineral Field (Fig. 1). The geology of the deposit has been described by Adams and Schmidt (1980) and de Roo (1989a, b). The deposit consist of two adjacent, vertical, pipe-like, massive sulphide orebodies. Above 98 m depth the ore is completely oxidised. The surface expression is limited to a small area of gossan float. The ore pipes are concentrically zoned and consists of three main types of mineralisation. In each pipe an outer sheath of siliceous ore envelopes a zone of massive pyritic ore, which in turn surrounds a central core of pyrrhotitic ore. Pyrrhotitic ore consists of massive to semi-massive sulphide (70–80% sulphide by volume), with up to 40% pyrrhotite. The pyrrhotite consists of intergrowths of monoclinic and intermediate pyrrhotite, with the monoclinic form predominant. The pyrrhotite grains are usually 20–50 μm in size, with rare grains up to 1 mm. The grains are equidimensional or slightly elongated, with the long axes preferentially aligned with the sulphide layering. Other constituents of the pyrrhotitic ore include Fe-rich sphalerite (~ 15%), galena (~ 10%), pyrite (~ 30%) and minor chalcopyrite and arsenopyrite in a gangue dominated by siderite (15–20%). Elura is hosted by a folded monotonous sequence of graded siltstones and shales belonging to the CSA Siltstone.

The Elura orebody produces a 45 nT bull's eye aeromagnetic high, ~ 500 m in diameter, which led to its discovery. Detailed aeromagnetic contours over Elura and the area immediately to the north are shown in Fig. 11. The magnetic response arises from the pyrrhotitic cores, compared to which the siliceous and pyritic ore types and the country rocks have negligible magnetisation (Emerson, 1980; Tonkin, 1985; Tonkin et al., 1988). Preliminary magnetic modelling and magnetic petrophysical studies of Elura have been described by Blackburn (1980) and Gidley and Hone (1980).

7. Magnetic properties of Elura ores and host rock

Twenty eight oriented block samples were collected from the Elura mine for the present study (16 pyrrhotitic ore, 4 pyritic ore, 4 siliceous ore and 4 host rock samples). Eight pyrrhotitic ore samples were taken along a 15 m E–W traverse at a depth of 241 m and a further eight along a 30 m E–W traverse 390 m below ground level. The other 12 samples came from a 45 m E–W traverse, at a depth of 231 m, from the centre of the main pyritic ore zone, through the siliceous ore envelope and into the host rock. Magnetic properties were measured as for the Magnetic Ridge study described above. Thermomagnetic analysis of a sample of pyrrhotitic ore showed that the pyrrhotite was mixed type, with ferrimagnetic monoclinic pyrrhotite and initially weakly magnetic (antiferromagnetic) intermediate pyrrhotite which underwent an irreversible transition to a ferrimagnetic phase above 200°C. The magnetic properties of the samples are summarised in Table 3. Fig. 12 shows the *NRM* directions of all specimens cut from the pyrrhotitic ore samples. The directions are well-grouped about a mean direction which is north and very steep up.

It is evident from Table 3 that only the pyrrhotitic ore contributes significantly to the magnetic anomaly at Elura. The magnetisation of the sampled main pyrrhotitic core is dominated by an intense and coherent remanence which is directed north and very steeply upwards. The two most weakly magnetic samples from the pyrrhotitic zone both came from the margins of the pyrrhotitic core and were found to consist of pyritic ore with minor pyrrhotite. The mean remanent intensity and mean bulk susceptibility of Table 3 correspond to a Koenigsberger ratio of 8.1, indicating that the rema-

Table 3
Bulk susceptibilities and *NRM*s of ores and host rock at Elura

Ore type	k (μG/Oe)	J (μG)	*NRM* direction
Pyrrhotitic ore	4900 ± 250)	22,700 ± 4000	(017°, −78°)
	(450–11,400)	(300–141,000)	(5°)
Pyritic ore	150	22 ± 10	(035°, −83°)
	(100–240)		(12°)
Siliceous ore	180	5 ± 1	(084°, −78°)
	(120–270)		(13°)
Host rock	15	< 1	–
	(5–29)		

Symbols as for Table 1.

nent magnetisation is an order of magnitude stronger than the induced magnetisation.

The susceptibility of the pyrrhotitic ore samples is markedly anisotropic, with an average anisotropy degree of 1.6. Fig. 13 shows the orientation of major axes and minor susceptibility axes. These stereoplots show that the magnetic fabric of the pyrrhotitic ore exhibits rotational symmetry about a subvertical magnetic lineation. The susceptibility anisotropy of the pyrrhotitic ore as a whole can be estimated as the tensorial mean of the susceptibility ellipsoids of the specimens. This is calculated by summing the tensors calculated from each susceptibility ellipsoid and dividing by their number. The major susceptibility of the pyrrhotitic ore is calculated as 6200 μG/Oe along an axis plunging 83° to 220°T. The susceptibility in the subhorizontal plane normal to this axis is effectively isotropic and equal to 4240 μG/Oe.

Elura has undergone a complex structural history, with four deformational events (D_{1-4}) interpreted from structures in the host rocks, three of which also affected the mineralisation (de Roo, 1989a, b). The deformations are associated with four distinct vertical axial plane cleavages, with different strikes. The two ore pipes formed during D_2 by metasomatism in the hinges of developing anticlinal domes. The shape and orientation of the main ore pipes, and of a number of mesoscopic replicas, reflect the vertically elongated D_2 strain ellipsoid. The present shape of the orebodies results from vertical stretching involving ductile shear of the sulphides. Vertical mineral lineations (L_2 and L_3, acquired during D_2 and D_3, respectively) within the host rocks also reflect this vertical stretching. The overall magnetic fabric of the Elura pyrrhotitic ore reflects preferred vertical orientation of basal planes of pyrrhotite crystals with *c*-axes randomly directed in the horizontal plane. Thus the magnetic fabric is consistent with the symmetry of the mesoscopic structures and the strain which produced them. The preferred orientation of pyrrhotite could have been produced by rotation of platy grains during vertical flow, by ductile deformation of individual grains or by preferential growth of vertically oriented crystals in a vertical stress field.

AF and thermal demagnetisation of specimens from the pyrrhotitic ore samples showed that the remanence is essentially monocomponent, with minor, randomly directed palaeomagnetic noise components picked up by exposure to magnetic fields during mining, sampling or sample preparation, superimposed on a dominant, consistently oriented component. Approximately 50% of the *NRM* intensity is demagnetised by 40–100 Oe (4–10 mT) AF. The dominant remanence component is not completely demagnetised below 200–300 Oe (20–30 mT) AF and ~320°C. AF and thermal cleaning gave essentially identical results. The mean direction of components (defined by Principal Component Analysis) for AF cleaning is $D=13°, I=-75°$ ($N=18$, $K=25.4$, $\alpha_{95}=7°$) and for thermal cleaning is $D=18°$, $I=-79°$ ($N=24$, $K=16.5$, $\alpha_{95}=8°$). These mean directions are both slightly steeper than the mean *NRM* direction, but all three mean directions are statistically indistinguishable. Thus the directions from all cleaned specimens may be combined to calculate the mean cleaned remanence direction: $D=17°$, $I=-78°$ ($N=42$, $K=19.7$, $\alpha_{95}=5°$). The cleaned remanence directions are significantly steeper than the present field direction (see Fig. 14). This fact, and the stability of the remanence up to the Curie temperature of pyrrhotite and to fairly strong alternating fields, imply that the *NRM* is not a recently acquired viscous remanent magnetisation (*VRM*). Since the present field in Australia is anomalously steep and *VRM* acquired since the last geomagnetic reversal, 0.7 Ma ago, should have largely averaged secular variation, a viscous rem-

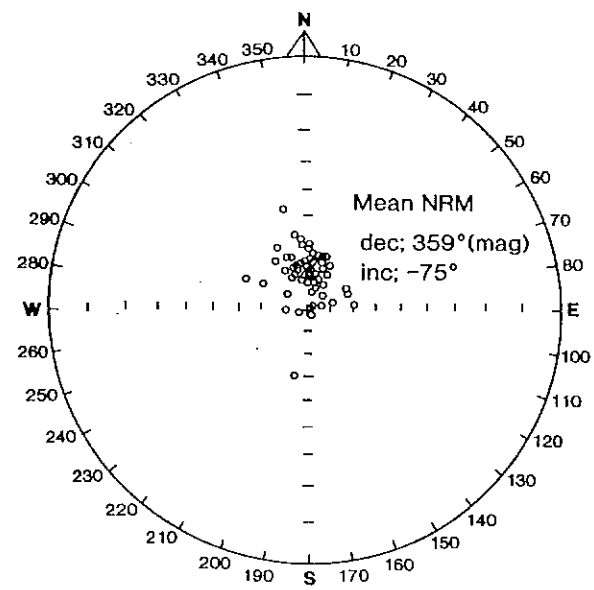

Fig. 12. *NRM* directions for all pyrrhotitic ore specimens from Elura. Equal-angle stereographic projection. The reference azimuth is magnetic north.

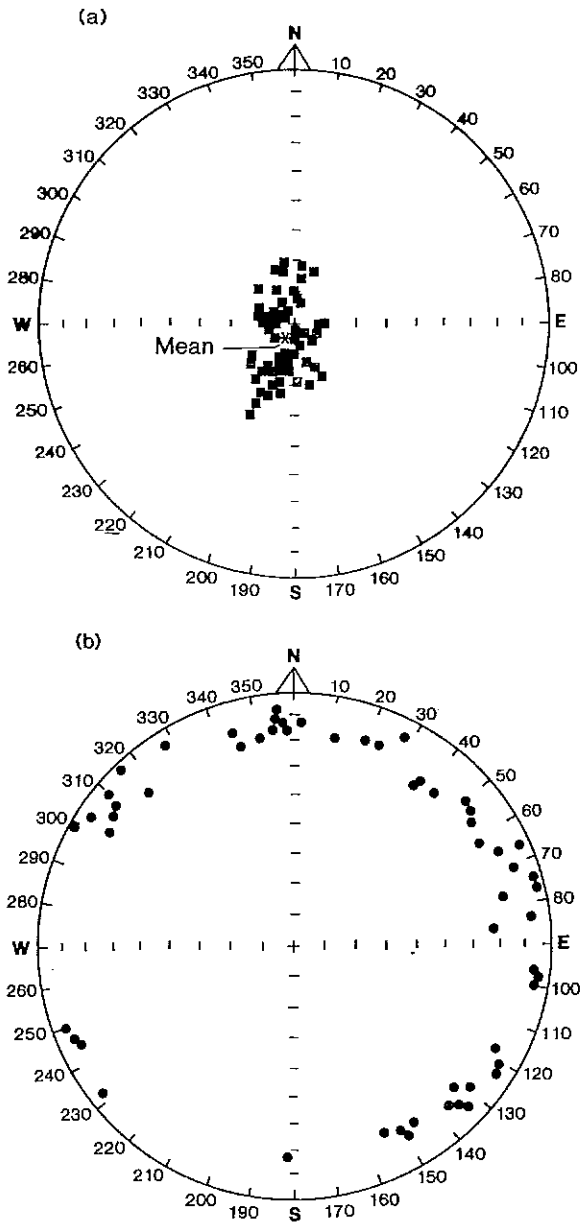

Fig. 13. Magnetic fabric of the Elura pyrrhotitic core. (a) Major susceptibility axes (magnetic lineations) of pyrrhotitic ore specimens. (b) Minor susceptibility axes (magnetic foliation poles) of Equal-area projection (Schmidt net). The reference azimuth is magnetic north.

anence is expected to be strongly biased towards the axial geocentric dipole field, which has a substantially shallower inclination of −50°. The *VRM* of very palaeomagnetically unstable grains, if present, may essentially track the present field. However, such grains should have very low unblocking temperatures and should be readily removed during initial thermal demagnetisation, thereafter revealing a shallower, longer term, *VRM*, followed by stable ancient components. There is no evidence of removal of progressively shallower components during thermal or AF cleaning. It follows that *VRM* overprinting of the remanence is negligible.

The time-averaging of secular variation may be partially counteracted by the magnetic anisotropy, which deflects the induced magnetisation and the *VRM*, if any, towards the subvertical major susceptibility axis. Thus *VRM* carried by the pyrrhotitic ore should have a direction intermediate between the dipole field and the induced magnetisation. It is clear from Fig. 14 that the remanence of the Elura pyrrhotitic ore is too steep to be of viscous origin, even when anisotropy is taken into account, and it is accordingly interpreted as an ancient component acquired during postmetamorphic cooling. The palaeomagnetic pole calculated from the mean cleaned direction is 53°S, 134°E ($dp = 9°$, $dm = 9°$). Assuming that the anisotropy of remanence acquisition at the blocking temperature is the same as the room temperature susceptibility anisotropy, the corrected estimate of the palaeofield direction is $D = 15°$, $I = -73°$, which corresponds to a pole position of 61°S, 130°E. The assumption regarding the anisotropy of remanence acquisition is based on the fact that anisotropy of weakly aligned assemblages of pyrrhotite grains, which have very high intrinsic anisotropy, depends only on the degree of preferred orientation and is essentially independent of the grain anisotropy. The corrected direction and pole are probably not grossly in error, because the deflection due to anisotropy is small in the present case, where the uncorrected remanence direction and the magnetic lineation only differ by 6°. The palaeopole position is consistent with a Carboniferous age of magnetisation and may represent cooling through the ~250°C isotherm at Elura. The older interpreted age of magnetisation at Elura, compared to the immediate Cobar area, and the absence of Mesozoic overprinting suggest that the Elura area was exhumed earlier. This is consistent with the geobarometric evidence discussed by Brill (1988).

8. Magnetic modelling at Elura

A ground magnetic survey carried out using a proton precession magnetometer, with measurements every 5

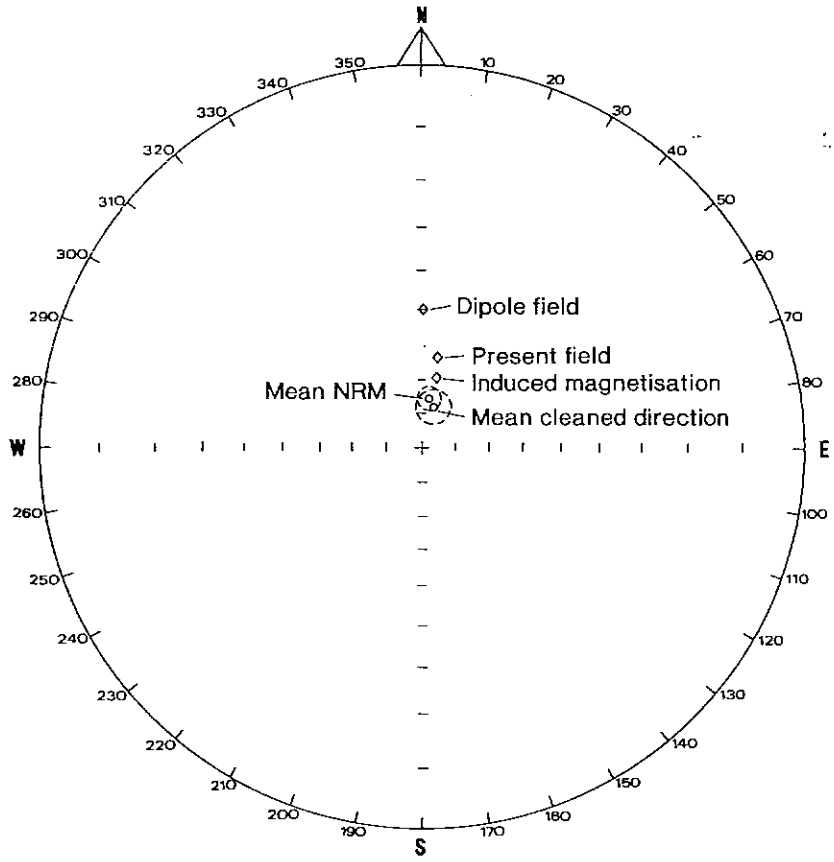

Fig. 14. Mean *NRM* and cleaned remanence directions for pyrrhotitic ore specimens from Elura, compared to the axial geocentric dipole field, the present field and the induced magnetisation directions. The reference azimuth is geographic north. The dashed circles represent 95% cones of confidence about the mean directions. Equal-angle stereographic projection.

m along traverses 25 m apart and a sensor height of 4.27 m, was used for comparison of theoretical and observed anomalies. The unusually large sensor height was chosen to reduce aliasing of the short wavelength, high-amplitude anomalies due to maghaemite-bearing pisolitic nodules in the soil, which are ubiquitous in the Cobar area. The prolate ellipsoid model of Emerson et al. (1985) was chosen as the most appropriate representation of the geometry of the Elura orebody. Two vertical prolate ellipsoids of revolution corresponding to the pyrrhotitic cores outlined by drilling were used for calculation of the theoretical ground magnetic anomaly over the orebody. The following magnetic properties, based on the properties of the pyrrhotitic ore samples were assumed to characterise the bulk magnetisation of the pyrrhotitic cores: *NRM* intensity = 2270 γ (22,700 mA/m), *NRM* declination = 8°, *NRM* inclination = −75°, major susceptibility = 6200 μG/Oe (77,910 × 10^{-6} SI), plunging at 83–220°, isotropic susceptibility of 4240 μG/Oe (53,280 × 10^{-6} SI) in the orthogonal plane. The effective Koenigsberger ratio is 6.4 when the anisotropy is taken into account. The regional geomagnetic field at Elura has intensity 57,100 γ (57,100 nT), declination 9.5° and inclination −62.5°.

The principal profile which passes over the centres of both ellipsoids is along geographic N–S. The predicted ground magnetic anomaly based on these magnetic properties and the initial assumed geometry matched the observed anomaly quite well. Small changes in the minor semiaxes of the ellipsoids produced a theoretical anomaly which fitted the observed anomaly very well, apart from short wavelength features arising from near-surface sources (Fig. 15). The local bumps in the measured profile of Fig. 15 clearly have a shallow origin and represent the effects of inhomogeneities in the subcropping gossan and in the maghaemite-rich soil. The final model provides a good

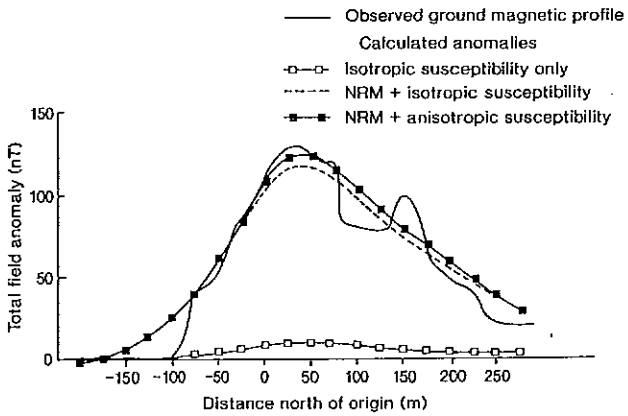

Fig. 15. Comparison of the observed ground magnetic anomaly with the anomaly calculated for the Elura orebody. The magnetic model represents the pyrrhotitic cores by vertical prolate ellipsoids of revolution, incorporating the measured magnetic properties.

representation of the actual form of the pyrrhotitic cores. The depth to the centres of both ellipsoids is 425 m, their N–S separation is 106 m, the larger southern ellipsoid has a major semiaxis of 325 m and minor semi-axes equal to 22.5 m, the northern ellipsoid has a major semi-axis of 125 m and minor semi-axes of 20 m.

The matching of the anomaly amplitude and its general form in Fig. 15 demonstrates that the magnetic properties of the orebody were well characterised by the sampling. Omitting remanence from the model gives a theoretical anomaly that is smaller than the observed anomaly by a factor of ~ 8. The effect of susceptibility anisotropy on the anomaly is small because of the dominance of remanence. Self-demagnetisation was also included in the analysis, but the effect is negligible for susceptibilities of this order. It can be firmly concluded, therefore, that the anomaly at Elura arises predominantly from the intense remanent magnetisation of the pyrrhotitic ore. In this case the remanence direction is subparallel to the induced magnetisation, but this is apparently coincidental, because there is strong evidence that the remanence is ancient. Australia has been in high latitudes from the Late Palaeozoic to the Middle Tertiary. Therefore, remanence of normal polarity acquired in this time interval will be directed steeply upwards, subparallel to the anomalously steep present field. Although the Elura anomaly could have been interpreted assuming magnetisation by induction, with a very high effective susceptibility, this assumption would be unjustified in general because the remanence of pyrrhotite-bearing orebodies may be oblique to the present field direction and of either polarity.

9. Conclusions

The magnetic anomaly at Magnetic Ridge has been shown to arise from a zone of disseminated monoclinic pyrrhotite, even though the susceptibility of the intersected horizon was much too low to produce the observed anomaly, rather than from a suspected unintersected source, possibly representing economically interesting mineralisation. The magnetisation of the pyrrhotite-bearing metasediments is dominated by remanence which is the sum of two ancient components, both oblique to the present field. The harder component, which is interpreted to be Triassic, has dual polarity and is overprinted by a softer component, of probable Mesozoic age, which has normal polarity but differs significantly in direction from the present field. Characterisation of the bulk remanence of the magnetic horizon at Magnetic Ridge was greatly assisted by palaeomagnetic cleaning, which enabled the complex distributions of *NRM* intensities and directions to be resolved into simple unimodal clusters of directions, corresponding to well-defined intensities, for each component. Quantitative modelling of the anomaly at Magnetic Ridge requires estimation of the magnetisation contrast between the zone of elevated pyrrhotite and the surrounding rocks, which have a background pyrrhotite concentration. The empirical relationship between susceptibility and remanence intensity for each polarity of hard remanence enables estimation of the contributions of paramagnetic minerals and of pyrrhotite to the total susceptibility and of the intrinsic Koenigsberger ratios of pyrrhotite grains for each type of *NRM*. The magnetic fabric at Magnetic Ridge exhibits a steep cleavage-parallel foliation and a down-dip lineation. The susceptibility ellipsoid is interpreted to be aligned with the strain ellipsoid in these rocks. The mean anisotropy degree is 1.45.

The magnetic anomaly of the Elura orebody arises solely from the vertical pipe-like cores of pyrrhotitic ore, which contain intergrown monoclinic and intermediate pyrrhotite. The magnetisation of the pyrrhotitic ore is dominated by remanence, directed steeply upwards, which is interpreted as an ancient metamor-

phic overprint magnetisation. The effective Koenigsberger ratio is 6.4, taking anisotropy into account. The pyrrhotitic ore exhibits a strong vertical magnetic lineation which reflects the deposition and deformation of the syndeformational orebody in a vertical stress field. There is no significant magnetic foliation on a macroscopic scale. The mean anisotropy degree is 1.46. Representing the pyrrhotitic cores as vertical prolate ellipsoids and using the measured magnetic properties for calculation of the theoretical anomaly gives a good match between the predicted and observed signatures of the Elura orebody. This confirms that the sampling has adequately characterised the bulk magnetic properties.

The two cases presented here, and many other examples, show that pyrrhotite-bearing rocks and ores often carry intense remanence, corresponding to high Koenigsberger ratios. Pyrrhotite, whilst easily thermally reset, is capable of retaining stable ancient remanence at ambient and slightly elevated temperatures. Thus the direction of remanence may make a large angle with the induced magnetisation, depending on the age of the pyrrhotite and the thermal history of the area. Modelling of magnetic anomalies due to pyrrhotite within particular provinces can be greatly assisted by palaeomagnetic studies of the remanence components carried by pyrrhotite-bearing rocks and by integrating this information with geological evidence regarding the genesis of pyrrhotite and thermal events in these areas. In some cases remanence directions carried by pyrrhotite may be inferred indirectly from geological information and the apparent polar wander path for the crustal block. The palaeomagnetic signatures of pyrrhotite-bearing rocks and ores can be sensitive recorders of relatively low grade thermal events and may provide useful information on thermal history. The magnetic fabric associated with preferred orientation of intrinsically highly anisotropic pyrrhotite grains is a sensitive indicator of deformation and can provide useful structural information.

Estimation of representative magnetic properties for modelling magnetic anomalies poses particular problems for pyrrhotite-bearing sources, because of the importance of remanence and, sometimes, susceptibility anisotropy. There may be large variations in *NRM* intensities and directions within the source region, reflecting multicomponent remanence and variable pyrrhotite content. The appropriate estimator of the bulk remanence of a macroscopically homogeneous, but mesoscopically heterogeneous, source that has been sampled representatively is the vectorial mean of the sample *NRM*s. Similarly, the susceptibility ellipsoid should be estimated by the tensorial mean of the sample susceptibility ellipsoids. There are no rigorous parametric statistical techniques for obtaining confidence limits on these estimates. The most promising approach to this important question of error bounds is development of nonparametric techniques, such as bootstrapping. This is currently being pursued in the CSIRO and elsewhere.

Acknowledgements

CRA Exploration Pty. Ltd. provided the magnetic survey data and the drill core samples from the Magnetic Ridge area. The Electrolytic Zinc Company of Australasia Ltd. provided access to the Elura Mine, assisted with sampling and provided the ground magnetic survey data used for the modelling. We thank Prof. Don Emerson for instigating the Elura study and Dr. Phil Schmidt and Dr. Mark Lackie for reading the manuscript.

References

Adams, R.L. and Schmidt, B.L., 1980. Geology of the Elura Zn–Pb–Ag deposit. In: D.W. Emerson (Editor), The Geophysics of the Elura Orebody, Cobar, New South Wales. Aust. Soc. Explor. Geophys., Sydney, pp. 1–4.

Baker, C.J., 1978. Geology of the Cobar 1:100,000 Sheet 8035. N.S.W. Geol. Surv., Sydney, 72 pp.

Blackburn, G., 1980. Gravity and magnetic surveys—Elura orebody. In: D.W. Emerson (Editor), The Geophysics of the Elura Orebody, Cobar, New South Wales. Aust. Soc. Explor. Geophys., Sydney, pp. 17–24.

Brill, B.A., 1988. Illite crystallinity, b_0 and Si content of K-white mica as indicators of metamorphic conditions in low-grade metamorphic rocks at Cobar, New South Wales. Aust. J. Earth Sci., 35: 295–302.

Clark, D.A., 1983. Magnetic Properties of Pyrrhotite—Applications to Geology and Geophysics. M.Sc. Thesis, University of Sydney, Sydney, 256 pp.

Clark, D.A., 1984. Hysteresis properties of sized dispersed monoclinic pyrrhotite grains. Geophys. Res. Lett., 11: 173–176.

Collinson, D.W., 1983. Methods in Rock Magnetism and Palaeomagnetism. Chapman and Hall, London, 503 pp.

De Roo, J.A., 1989a. The Elura Ag–Pb–Zn mine in Australia—ore genesis in a slate belt by syndeformational metasomatism along hydrothermal fluid conduits. Econ. Geol., 84: 256–278.

De Roo, J.A., 1989b. Mass transfer and preferred orientation development during extensional microcracking in slate-belt folds, Elura mine, Australia. J. Metamorph. Geol., 7: 311–322.

Dekkers, M.J., 1988. Magnetic properties of natural pyrrhotite Part I: Behaviour of initial susceptibility and saturation-magnetization-related rock-magnetic parameters in a grain-size dependent framework. Phys. Earth Planet. Inter., 52: 376–393.

Embleton, B.J.J., 1981. A review of the paleomagnetism of Australia and Antarctica. In: M.W. McElhinny and D.A. Valencio (Editors), Paleoreconstruction of the Continents. Am. Geophys. Union Geodyn. Ser., 2: 77–92.

Emerson, D.W., 1980 (Editor). The Geophysics of the Elura Orebody, Cobar, New South Wales. Aust. Soc. Explor. Geophys., Sydney, 205 pp.

Emerson, D.W., Clark, D.A. and Saul, S.J., 1985. Magnetic exploration models incorporating remanence, demagnetization and anisotropy: HP 41C handheld computer algorithms. Explor. Geophys., 16: 1–122.

Fisher, R.A., 1953. Dispersion of a sphere. Proc. R. Soc. London A, 217–295–305.

Gidley, P.R. and Stuart, D.C., 1980. Magnetic property studies and magnetic surveys of the Elura Prospect, Cobar, NSW. In: D.W. Emerson (Editor), The Geophysics of the Elura Orebody, Cobar, New South Wales. Aust. Soc. Explor. Geophys., Sydney, pp. 25–35.

Glen, R.A., 1987. Copper- and gold-rich deposits in deformed turbidites at Cobar, Australia: their structural control and hydrothermal origin. Econ. Geol., 82: 124–140.

Glen, R.A., Dallmeyer, R.D. and Black, L.P., 1986. Preliminary report on new isotopic evidence for, and implications of, an Early Devonian deformation at Cobar. N.S.W. Geol. Surv. Q. Notes, 64: 26–30.

Hone, I.G. and Gidley, P.R., 1986. Investigation of the characteristics and source of the Magnetic Ridge magnetic anomaly, Cobar, NSW. Bur. Miner. Resour. Geol. Geophys. Rep., 248.

Kirschvink, J.L., 1980. The least-squares line and plane and the analysis of palaeomagnetic data. Geophys. J.R. Astron. Soc., 62: 699–718.

Kropacek, V., 1971. Distribution of the values of natural remanent magnetization and magnetic susceptibility of some minerals. Stud. Geophys. Geodaet., 15: 340–352.

Kropacek, V. and Krs, M., 1971. Magnetism of natural pyrrhotite, haematite and ilmenite. Stud. Geophys. Geodaet., 15: 161–172.

Pogson, D.J. and Hillyard, D., 1981. Results of isotopic age dating related to Geological Survey of New South Wales investigations, 1974–1978. Geol. Surv. N.S.W. Rec., 20(2): 251–273.

Power, L.F. and Fine, H.A., 1976. The iron–sulphur system. Part I. The structure and physical properties of the compounds of the low-temperature phase fields. Miner. Sci. Eng., 8: 106–128.

Ribbe, P.H., 1974 (Editor). Sulfide Mineralogy. Mineral. Soc. Am., Washington, DC, Short Course Notes, Vol. 1, 284 pp.

Ridley, B.H. and Brown, H.E., 1980. The transformer bridge and magnetic susceptibility measurement. Bull. Aust. Soc. Explor. Geophys., 11: 110–114.

Schwarz, E.J., 1974. Magnetic properties of pyrrhotite and their use in applied geology and geophysics. Geol. Surv. Can. Pap., 74-59, 24 pp.

Schwarz, E.J. and Vaughan, D.J., 1972. Magnetic phase relations of pyrrhotite. J. Geomagn. Geoelectr., 24: 441–458.

Shuey, R.T., 1975. Semiconducting Ore Minerals. Elsevier, Amsterdam, 415 pp.

Tonkin, C., 1985. The magnetisation of the Elura orebody, Cobar, N.S.W. B.Sc. (Hons) Thesis. Univ. Sydney, Sydney, 161 pp.

Tonkin, C., Clark, D.A. and Emerson, D.W., 1988. The magnetisation of the Elura orebody, Cobar, NSW. Explor. Geophys., 19: 368–370.

Vaughan, D.J. and Craig, J.R., 1978. Mineral Chemistry of Metal Sulfides. Cambridge Univ. Press, Cambridge, 493 pp.

Ward, J.C., 1970. The structure and properties of some iron sulphides. Rev. Pure Appl. Chem., 20: 175–206.